

An Investigation of Strain-Softening Phenomenon in Al–0.1% Mg Alloy during High-Pressure Torsion Processing

Yi Huang,* Justine Millet, Nian X. Zhang, Péter Jenei, Jenő Gubicza, and Terence G. Langdon

An Al–0.1% Mg alloy is processed by high-pressure torsion (HPT) at room temperature. The Al–0.1% Mg alloy displays strain-softening phenomenon through hardness evolution: the hardness values in the disc center area are higher than at the disc edge area after 1/2, 1, and 3 turns, and the size of the hard region in the disc center gradually reduces as the number of turns increases from 1/2 to 3 turns. The hardness values evolve toward homogeneity along the disc diameters after 5 and 10 turns. Electron backscatter diffraction (EBSD) and X-ray line profile analysis suggest that the lower hardness values at the disc edge area in the Al–0.1% Mg alloy are related to a recovery/recrystallization mechanism where the material is subjected to heavy straining.

1. Introduction

Severe plastic deformation (SPD) has been shown to effectively produce ultrafine-grained (UFG) materials by applying very high strain to the bulk material.^[1] As one of the most efficient SPD techniques, high-pressure torsion (HPT) can achieve significant grain refinement and strength enhancement in

HPT-processed metallic materials.^[2] A wide range of metals and alloys have been successfully processed by HPT, such as Al and Al alloys,^[3–7] Cu and Cu alloys,^[8–11] Mg and Mg alloys,^[12–14] Ti and Ti alloys,^[15–17] and steel.^[18–20] In practice, different materials display different hardness evolutions during HPT processing. Thus, the hardness evolution during HPT processing follows three different models observed to date:^[21,22] 1) microhardness evolution with no recovery in most metals and alloys; 2) microhardness evolution with softening in some materials with high stacking-fault energy (SFE;

such as high purity Al); 3) microhardness evolution with weakening in some pure metals and two-phase alloys (such as Pb, Zn–Al, and Pb–Sn alloys).

It was reported that in high-purity Al, the very high SFE leads to easy cross-slip and rapid microstructural recovery.^[3] Therefore, the hardness distribution along the disc diameter after a lower number of HPT turns gives a bell-shaped curve. This means there is a higher hardness value in the disc center area but a lower hardness value in disc edge area, thereby demonstrating the occurrence of a strain-softening phenomenon before the hardness values become reasonably homogeneous along the disc diameter after high numbers of HPT turns. However, there are no reports providing an explanation for the reason that the breadth of the bell-shaped curve of higher hardness values gradually decreases with increasing numbers of HPT turns until the hardness achieves a homogeneous distribution across the disc diameter after high numbers of turns.


High-purity Al is very soft and has only limited engineering applications so that the element Mg is added to pure Al to form solid solution strengthened Al–Mg alloys which are then used in various applications in transportation, packaging, and general engineering industries.^[23] The equilibrium solubility of Mg in the Al matrix at room temperature (RT) is $\approx 1.6\%$ Mg (all compositions in this report expressed in weight percentage)^[24] and it provides the most effective enhancement of strength among all alloying additions in the aluminum solid solution.^[25] The strength of Al–Mg alloys increases strongly with the addition of Mg. Research reported on the HPT processing of Al–Mg alloys shows that Al–5% Mg and Al–1% Mg alloys have similar hardness evolution models with lower hardness values in the disc center area but higher hardness values in the disc edge area showing microhardness evolution with no recovery.^[26,27] In contrast, it has been shown that in HPT-processed Al–0.1%

Dr. Y. Huang
Department of Design and Engineering
Faculty of Science and Technology
Bournemouth University
Poole, Dorset BH12 5BB, UK
E-mail: yhuang2@bournemouth.ac.uk

Dr. Y. Huang, Dr. N. X. Zhang, Prof. T. G. Langdon
Materials Research Group
Department of Mechanical Engineering
University of Southampton
Southampton SO17 1BJ, UK

J. Millet
Phelma – School of Engineering in Physics, Electronics and Materials
Grenoble INP Minatéc
3 Parvis Louis Neel, BP 257, 38016 Grenoble Cedex 1, France

Dr. P. Jenei, Prof. J. Gubicza
Department of Materials Physics
Eötvös Loránd University
PO Box 32, Budapest H-1518, Hungary

 The ORCID identification number(s) for the author(s) of this article can be found under <https://doi.org/10.1002/adem.201901578>.

© 2020 The Authors. Published by Wiley-VCH GmbH. This is an open access article under the terms of the Creative Commons Attribution-NonCommercial-NoDerivs License, which permits use and distribution in any medium, provided the original work is properly cited, the use is non-commercial and no modifications or adaptations are made.

DOI: 10.1002/adem.201901578

Mg alloy, the hardness evolution displays a strain-softening phenomenon at low numbers of HPT turns.^[28]

Pure Al has a high SFE ($\approx 200 \text{ mJ m}^{-2}$),^[29] whereas Mg has a relatively high value of the SFE ($\approx 125 \text{ mJ m}^{-2}$).^[30] Theoretical calculations demonstrate that upon the addition of Mg to Al, the SFE decreases linearly in the Al–Mg system.^[31] Although HPT-processed high-purity Al and Al–0.1% Mg alloy exhibit similar hardness evolution models with strain softening at lower numbers of HPT turns, recognizing that there may be a difference in SFE between these two systems, it is accordingly imperative to conduct a microstructural analysis and to correlate the microstructure with the hardness evolution in the Al–0.1% Mg alloy. Therefore, this research was initiated to investigate the mechanism governing the strain-softening phenomenon in an HPT-processed Al–0.1% Mg alloy and to identify the reason that the breadth of the bell-shaped curve

of higher hardness values gradually decreases with the increase in HPT turns.

2. Results

2.1. Microstructure Development during HPT Processing

The as-annealed Al–0.1% Mg alloy had a very coarse grain size of $\approx 2200 \mu\text{m}$ and a low hardness value of $\approx 18.1 \text{ Hv}$. The microstructures of the HPT-processed Al–0.1% Mg alloy are shown in **Figure 1**, where black lines represent high-angle grain boundaries (HAGBs, defined as misorientations $>15^\circ$) and golden lines represent low-angle grain boundaries (LAGBs, defined as misorientations in the range of 2° – 15°). The grain boundaries were determined with the threshold value of misorientation

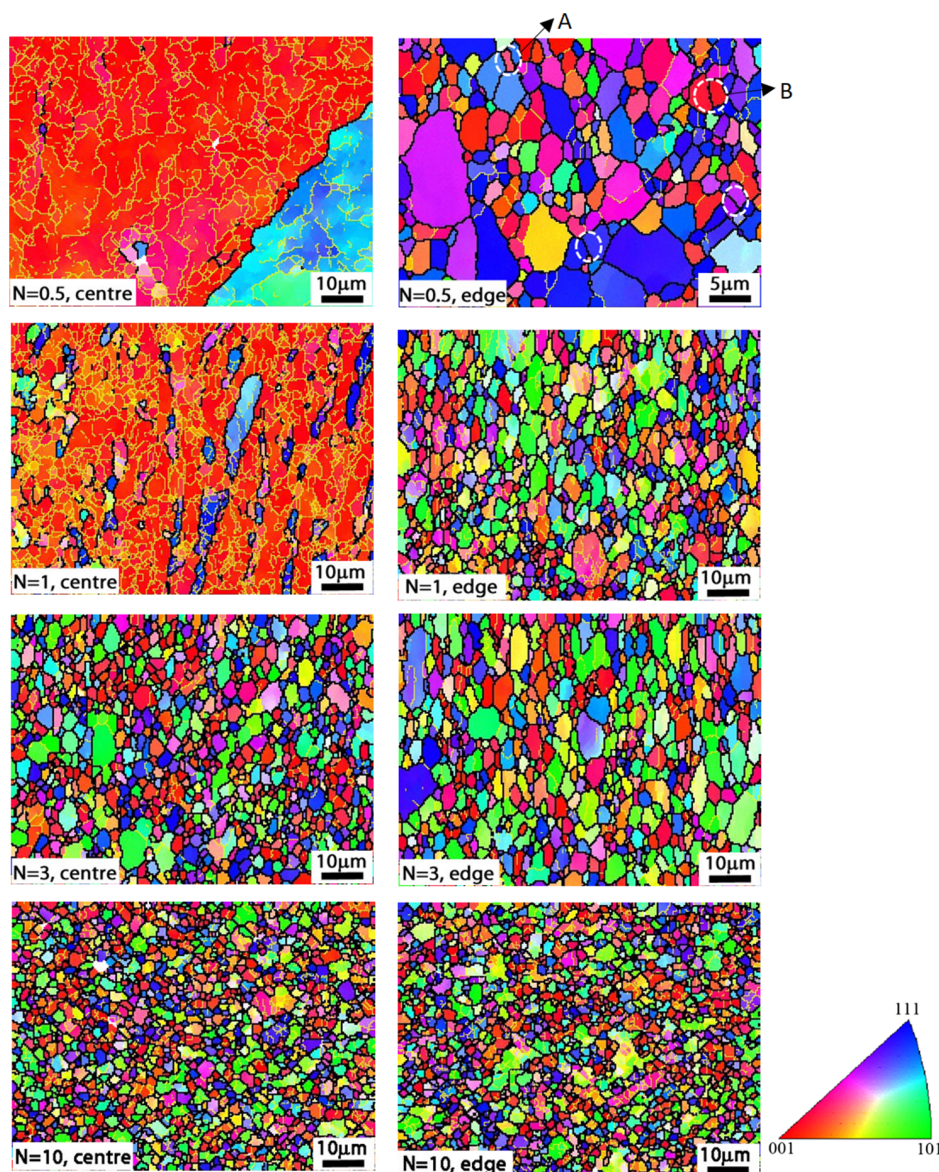


Figure 1. Microstructures in Al–0.1% Mg alloy after 1/2, 1, 3, 10 turns in disc center (left) and edge area (right).

angle above 15°. The grain sizes in this report are the mean values from the grain size distribution detected by EBSD. In Figure 1, the left and right column images correspond to the microstructures in the discs at the center and edge areas after HPT processing to 1/2, 1, 3, and 10 turns.

Inspection shows that there is significant grain refinement at the disc edge area even after 1/2 turn where the grain size is reduced from an initial value of $\approx 2200 \mu\text{m}$ to a value of $\approx 3.1 \mu\text{m}$. In contrast, in the disc center area after 1/2 turn, there is no significant grain refinement but many subgrains are visible within the coarse grains. After 1 turn, there is little additional grain refinement at the disc edge area with an average grain size of $\approx 2.5 \mu\text{m}$, whereas in the disc center area after 1 turn there are some fine grains which start to form within the coarse grains but there is no evidence for homogeneous grain refinement at this early stage. Further torsional straining to 3 turns leads to grain refinement at both the disc center and edge areas with average grain sizes of ≈ 2.1 and $2.6 \mu\text{m}$ in the center and edge areas, respectively. Finally, after 10 turns, there is a homogeneous grain refinement in both the center and edge areas with similar average grain sizes of $\approx 1.9 \mu\text{m}$.

Table 1 shows the EBSD misorientation data for discs processed to 1/2, 1, 3, and 10 turns. After 1/2 turn of HPT, there is a very high fraction of $\approx 91.4\%$ of HAGBs in the disc edge area and a very high fraction of $\approx 90.4\%$ of LAGBs in the disc center area. However, as the number of turns increases to 1 turn, the disc edge area maintains a relatively high fraction of HAGBs of $\approx 78.9\%$, whereas the fraction of HAGBs in the disc center area increases to $\approx 34.3\%$. Further application of torsional straining to 3 turns leads to a high fraction of HAGBs in both the disc center and edge areas with measured values of $\approx 91.6\%$ and $\approx 89.8\%$, respectively. After 10 turns, both the disc center and the edge areas have very similar high fractions of HAGBs at $\approx 79.8\%$ and 77.7% , respectively. The evolutions of the fractions of HAGBs with different numbers of HPT turns shown in Table 1 provide a close match to the corresponding microstructural features shown in Figure 1.

The fractional values of the different grain boundary characters in samples processed to 1/2, 1, 3, and 10 turns are shown schematically in Figure 2. The three sets of grain boundary characters are LAGBs (labeled as $2-15^\circ$ grain boundary character in Figure 2), $\Sigma 3$ twin boundaries, and HAGBs without $\Sigma 3$ twin boundaries (labeled as $>15^\circ$ grain boundary character in Figure 2). The appearances of some twins in the disc edge area of the 1/2 turn sample in Al–0.1% Mg alloy are highlighted by white circles bordered by dashed line in Figure 1. The circle marked as A is an obvious twin with a twinning section having

Table 1. Fractions of LAGBs and HAGBs in disc centers and edges after different numbers of HPT turns.

| Number of turns | Disc center area | | Disc edge area | |
|-----------------|------------------|-----------|----------------|-----------|
| | LAGBs [%] | HAGBs [%] | LAGBs [%] | HAGBs [%] |
| $N = 0.5$ | 90.4 | 9.6 | 8.6 | 91.4 |
| $N = 1$ | 65.7 | 34.3 | 21.1 | 78.9 |
| $N = 3$ | 8.4 | 91.6 | 10.2 | 89.8 |
| $N = 10$ | 20.2 | 79.8 | 22.3 | 77.7 |

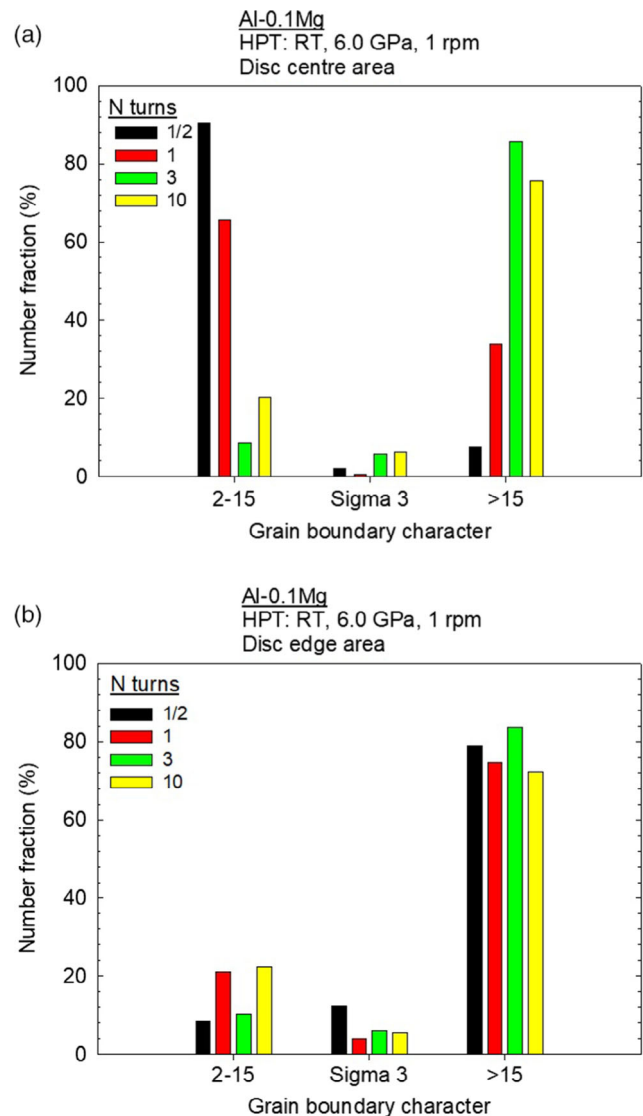


Figure 2. Grain boundary character distributions for the disc processed through 1/2, 1, 3, and 10 turns at a) disc center area and b) disc edge area.

different orientations with the grain so that the twin has a different color from the grain color. The circle marked as B is twinning that can be easily neglected because the width of the twin is so small that the orientation of twinning cannot be viewed properly in the image with the current image magnification so that the twin marked as B appears as a black line in the image. But on the left side and right side of the black line, the grain has the same orientation (pink color) and this confirms the black line marked as B is a twin within a grain. Several twins with small twinning width are also marked in white circles in the same image of the disc edge area of the 1/2 turn sample in Figure 1. For the 1/2 turn sample, the disc edge has $\approx 12.4\%$ $\Sigma 3$ twin boundaries which is significantly higher than the $\approx 1.9\%$ $\Sigma 3$ twin boundaries at the disc center area. As the number of turns increases to 1 turn, the fractions of $\Sigma 3$ twin boundaries at the disc edge and center are $\approx 4.1\%$ and $\approx 0.4\%$, respectively. Further increases in the number of turns to 3 and 10 turns give

fractions of $\Sigma 3$ twin boundaries that lie at similar levels for both center and edge areas. The fraction of $\Sigma 3$ twin boundaries in the disc center and edge areas are 5.8% and 6.0% for the 3 turns sample and 6.3% and 5.5% for the 10 turns sample.

2.2. Hardness Evolution in Al-0.1% Mg Alloy during HPT Processing

The evolution in hardness with increasing numbers of HPT turns in the Al-0.1% Mg alloy is shown in **Figure 3**. Inspections of the hardness development in Figure 3 shows that the centers of the discs exhibit higher values, rather than lower values, compared with the disc edge area after 1/2, 1, and 3 turns but the hardness distribution tends to become homogeneous after 5 and 10 turns. Overall, the hardness increases from an initial as-annealed value of ≈ 18.1 to ≈ 30 Hv in Al-0.1% Mg after 10 turns of HPT processing.

Further inspection of Figure 3 shows that the breadth of the bell-shaped curve of the higher hardness values along the disc diameter span from -3 to $+3$ mm for the 1/2 turn sample as demonstrated by the blue dual arrow line. The green dual arrow line and pink dual arrow line in Figure 3 describe the breadths of the bell-shaped curves varying from -1.5 to $+1.5$ mm for the 1 turn sample and from -0.6 to $+0.6$ mm for the 3 turns sample. Overall, the breadth of the bell-shaped curves in Figure 3 gradually decreases as the number of turns increases from 1/2 to 1 and 3 turns and thereafter there is no evidence for a bell-shaped curve.

2.3. Microstructural Results from the X-Ray Line Profile Analysis

To reveal the reason for the different hardness evolutions for low and high numbers of turns, the crystallite size and the dislocation density were determined from the X-ray line profile analysis for the lowest (1/2) and highest (10) numbers of turns. **Table 2** shows the results for the center and edge parts of the

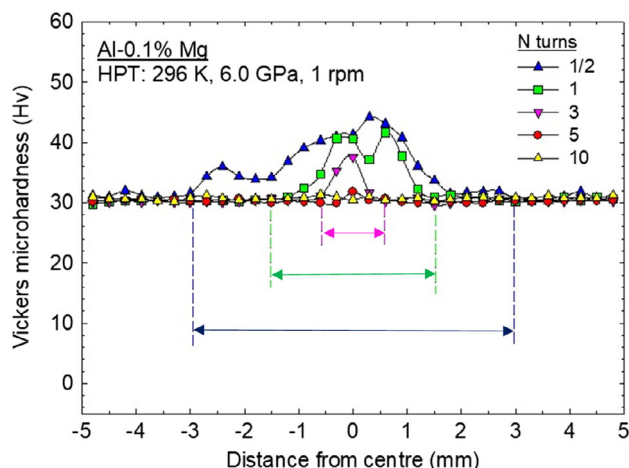


Figure 3. Distribution of Vickers microhardness, Hv, along the diameters of discs processed by HPT through 1/2, 1, 3, 5, and 10 turns in Al-0.1% Mg alloy; the blue, green, and pink dual arrow lines demonstrate the breadth of the bell-shaped curves for samples after 1/2, 1, and 3 turns.

Table 2. The dislocation density (ρ) obtained by X-ray line profile analysis.

| Sample | Dislocation density ρ [10^{14} m^{-2}] |
|------------------|---|
| 1/2 turn, center | 2.9 ± 0.3 |
| 1/2 turn, edge | 1.1 ± 0.3 |
| 10 turns, center | 1.4 ± 0.3 |
| 10 turns, edge | 0.9 ± 0.3 |

discs processed for 1/2 and 10 turns. For all investigated samples and locations, the crystallite size values were close to the detection limit of the present diffraction system (about 1000 nm); therefore, they are not shown and interpreted here. For the 1/2 turn sample, the disc edge area has a lower dislocation density of $(1.1 \pm 0.3) \times 10^{14} \text{ m}^{-2}$ than the dislocation density of $(2.9 \pm 0.3) \times 10^{14} \text{ m}^{-2}$ at the disc center area after 1/2 turn. For the 10 turns sample, the dislocation density in the disc center area is similarly low ($(0.9 \pm 0.3) \times 10^{14} \text{ m}^{-2}$) as the dislocation density at the center area ($(1.4 \pm 0.3) \times 10^{14} \text{ m}^{-2}$).

3. Discussion

Examining the grain structure evolution in the disc center area from 1/2, 1, 3, and 10 turns in the left column of Figure 1, it is noted that many subgrains formed within the coarse grain in the 1/2 turn sample but new grain boundaries started to form from these cellular structures in the 1 turn sample. Gradually, these cellular structures fully evolved into UFG structures in the 3 and 10 turns samples. These observations confirmed the mechanism of new grains formation during heavy shear deformation as also reported in Armco iron^[32] and 2219 aluminum alloy.^[33]

Inspection of the microstructure in the edge area of the 1/2 turn sample in Figure 1 shows that within each individual grain there are few dislocations or LAGBs and these features are essentially similar to the microstructure observed after an initial annealing heat treatment. But the grain size at the disc edge area after 1/2 turn is $\approx 3.1 \mu\text{m}$ and this is much smaller than the grain size of the initial as-annealed state which is $\approx 2200 \mu\text{m}$. The misorientation data of the edge area of the 1/2 turn sample in Table 1 show that the number of fractions of the LAGBs and HAGBs is $\approx 8.6\%$ and $\approx 91.4\%$, respectively. The $\approx 91.4\%$ of HAGBs in the disc edge area in the Al-0.1% Mg alloy after 1/2 turn is much higher than the value of $\approx 80\text{--}85\%$ which is achieved in most HPT-processed materials up to 1/2 and 1 turns.^[6,7,26,27] The fraction of $\Sigma 3$ twin boundaries in the edge area of the 1/2 turn sample shown in Figure 2b is $\approx 12.4\%$.

In face-centered cubic (FCC) metals, the most important coincident site lattice (CSL) boundary $\Sigma 3$ is dominated by the formation of annealing twins.^[34] Annealing twins in high-purity Al with high SFE were reported by in situ EBSD observations.^[35] A recent investigation on the microstructure of the deformed and annealed commercial purity Al-1050 alloy demonstrated the existence of a $\Sigma 3$ boundary evolved from a recrystallization twin.^[36] The microstructural features of a high fraction of HAGBs and a high fraction of $\Sigma 3$ twin boundaries in Al-1% Mg alloy suggest that dynamic recrystallization occurred in the disc edge area and this produced a lower hardness at the edge area, whereas dislocation strengthening appears to be the

mechanism for the higher hardness in the disc center area in the 1/2 turn sample. Figure 1 shows that the disc edge area of the 1/2 turn sample has a much smaller grain size ($\approx 3.1 \mu\text{m}$) compared with the disc center area, whereas Table 2 shows that the disc edge area has a two times lower dislocation density than in the disc center area. The disc edge and center areas have dislocation densities of $\approx (1.1 \pm 0.3) \times 10^{14} \text{ m}^{-2}$ and $\approx (2.9 \pm 0.3) \times 10^{14} \text{ m}^{-2}$, respectively, in the 1/2 turn sample. The results for the dislocation density in the 1/2 turn sample shown in Table 2 provide additional evidence that dynamic recrystallization occurred in the disc edge area.

A temperature rise during HPT processing is a factor that may produce recovery and recrystallization in addition to the plastic strain applied on the material. Several reports investigated the temperature rise due to heat generated during plastic deformation and friction inherent in the material flow during the anvil rotation through finite element modeling.^[37–39] Recent investigations examined the temperature rise and corresponding microstructure changes in Al, Ag, and Cu during HPT processing and it was concluded that the temperature rise is of only minor significance in initiating dynamic recrystallization.^[40,41] Accordingly, the recrystallization phenomenon in Al–0.1% Mg alloy appears to be mainly due to the formation of large fractions of lattice defects from the heavy shear strains.

During HPT processing, the equivalent von Mises strain, ϵ_{eq} , imposed on the disc is given by the relationship^[32]

$$\epsilon_{\text{eq}} = \frac{2\pi Nr}{h\sqrt{3}} \quad (1)$$

where N is the number of HPT turns, r is the radial distance from the center of the disc, and h is the initial height of the disc.

Figure 3 shows that lower numbers of turns of HPT processing, such as 1/2, 1, and 3 turns, give bell-shaped curves of high hardness values along the disc diameter, and the breadth of these bell-shaped curves decrease with increasing numbers of HPT turns. For the $N=1/2$ turn sample, the breadth of the bell-shaped curve extends from -3 to $+3$ mm as shown in Figure 3. Using $r=3$ mm in Equation (1), a calculated equivalent strain of $\epsilon_{\text{eq}}=6.4$ should be the critical strain to incur recrystallization in the 1/2 turn sample so that when the equivalent strain along the disc diameter is above this critical strain then recrystallization will occur. For the 1/2 turn sample, the calculated equivalent strain of $\epsilon_{\text{eq}}=6.4$ also means that when the radial distance r reaches a critical value of $r > 3$ mm so recrystallization will occur in the area from $r=3$ mm to the disc edge and this will produce a lower hardness. It will also lead to a low dislocation density, a high fraction of HAGBs and a high fraction of $\Sigma 3$ twin boundaries in the recrystallization area.

The calculated critical strain of 6.4 that may incur recrystallization in the 1/2 turn sample is also the critical strain that will induce recrystallization in the $N=1$ and $N=3$ turns samples. For the $N=1$ turn sample, applying a critical strain value of 6.4 in Equation (1), then the calculated value of r should represent the critical position along the disc diameter where recrystallization can occur. A calculated value of $r=1.5$ mm for the 1 turn sample matches the breadth of the bell-shaped curve shown in Figure 3 which means that when $r > 1.5$ mm recrystallization occurs in the area from $r=1.5$ mm to the disc edge. Applying the same

critical strain value of 6.4 in Equation (1) for the $N=3$ turns sample leads to a calculated value of $r=0.6$ mm which is almost the same breadth as the bell-shaped curve in Figure 3. This means when $r > 0.6$ mm, recrystallization occurs in the area from $r=0.6$ mm to the disc edge. When a torsional straining to $N=5$ and $N=10$ turns is imposed on the sample, applying the critical strain value of 6.4 in Equation (1) produces calculated values of $r=0.3$ mm and $r=0.15$ mm for these two levels of straining, respectively. These critical values of r of 0.3 and 0.15 mm are exceptionally small so that almost the whole disc surface exhibits recrystallization in the 5 and 10 turns samples. These calculations provide an explanation for the development of a homogenous hardness distribution in the 5 and 10 turns samples as shown in Figure 3 and they are consistent with the relatively low dislocation density in the 10 turns sample as recorded in Table 2.

These calculations may be illustrated as shown in Figure 4 where the critical value of r , corresponding to the critical strain of 6.4, is plotted against the different numbers of HPT turns and, in addition, the large discs provide schematic illustrations of the gradual evolution of the recrystallized region on the disc surface. Thus, in Figure 4, the schematic discs symbolize the surface of the HPT-processed discs with the red area in the disc outer region corresponding to the area of recrystallization and the inner gray region representing the unrecrystallized area. The illustrations show that the critical r value decreases as the number of HPT turns increases. Thus, as the numbers of turns increases from 1/2 to 1 and 3 turns, the critical r value decreases from ≈ 3 to ≈ 1.5 and ≈ 0.6 mm to the disc edge for these three conditions, respectively. For 5 and 10 turns, the critical r values are only ≈ 0.3 and ≈ 0.15 mm, respectively. Thus, the schematic discs in Figure 4 show an overall view of the evolution in the recrystallization area with different numbers of HPT turns so that the gray area at the disc center gradually decreases with increasing numbers of HPT turns and the red area at the outer region of the disc gradually increases

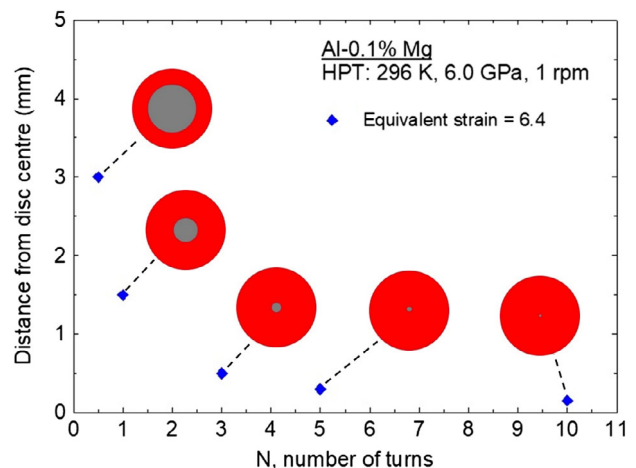


Figure 4. Schematic illustration of critical value of r versus number of HPT turns and the demonstration of recrystallized region evolution with different numbers of turns; red and gray areas represent the recrystallization and unrecrystallized regions in the HPT-processed discs, respectively.

with increasing numbers of turns. In practice, after 5 and 10 turns, the disc center area corresponds to a very small unrecrystallized region which was not detected by the hardness measurements and instead the disc surface contained a relatively large recrystallized region corresponding to a homogenous hardness distribution. This approach, therefore, provides an excellent explanation for the decrease in the breadths of the bell-shaped curves shown in the hardness distributions shown in Figure 3.

The mechanism of strain-softening in the Al–0.1% Mg alloy is different from that in high-purity Al. For high-purity Al, the strain softening is attributed to the easy cross-slip and rapid microstructural recovery due to the high SFE.^[3–7] For Al–0.1% Mg alloy, the SFE is slightly lower than high-purity Al; therefore, it may have a different strain-softening mechanism. From EBSD, X-ray and hardness measurements, and the preceding analysis on HPT-processed Al–0.1% Mg samples, it was confirmed that dynamic recrystallization first occurred in the disc edge area at lower numbers of turns, then gradually spread toward the disc center area at higher numbers of turns. The spread of the dynamic recrystallization regions from the disc edge area toward the center area caused the strain-softening phenomenon in the Al–0.1% Mg alloy during HPT processing.

4. Conclusions

The hardness distribution of an HPT-processed Al–0.1% Mg alloy shows a strain-softening phenomenon in the form of bell-shaped curves after 1/2, 1, and 3 turns but conversely displays homogenous hardness distribution after 5 and 10 turns.

An EBSD analysis of the edge area of the 1/2 turn sample shows a refined grain size of $\approx 3.1 \mu\text{m}$ and high fractions of HAGBs ($\approx 91.4\%$) and $\Sigma 3$ twin boundaries ($\approx 12.4\%$). An X-ray line profile analysis on the edge area of the 1/2 turn sample gave a much lower dislocation density of $\approx (1.1 \pm 0.3) \times 10^{14} \text{ m}^{-2}$ than in the center part ($(2.9 \pm 0.3) \times 10^{14} \text{ m}^{-2}$). At the same time, for 10 turns, a low dislocation density ($(0.9\text{--}1.4) \times 10^{14} \text{ m}^{-2}$) was measured at both the center and the edge of the disc.

Plots of hardness against distance from the center of the HPT disc show a bell-shaped curve at low numbers of turns but with the breadth of the bell-shaped curve gradually decreasing with increasing numbers of turns. This is explained by noting that dynamic recrystallization occurs during HPT processing and the total region of recrystallization around the periphery of the disc gradually increases with increasing numbers of HPT turns.

5. Experimental Section

The experiments were conducted using a commercial purity Al–0.1% Mg alloy containing 0.003% Si and 0.001% Fe as minor impurities. The alloy was received in the form of extruded rods having diameters of 13 mm. These rods were first annealed for 1 h at 773 K and then the rods were machined to reduce the diameters to 9.95 mm and sliced into discs with thicknesses of ≈ 1.2 mm. These sliced discs were ground with 800 grit papers to final thicknesses of ≈ 0.85 mm. The HPT processing was conducted at RT under quasiconstrained conditions^[37,42] through total numbers of turns, N , of 1/2, 1, 3, 5, and 10. The HPT operation used an imposed pressure of 6.0 GPa and a rotational speed of 1 rpm.

After HPT processing, the samples were ground with abrasive paper, then polished on cloth with diamond paste, and a final polishing was performed using a colloidal silica solution. The Vickers microhardness, H_v ,

was measured on polished disc surfaces using an FM300 microhardness tester equipped with a Vickers indenter. Each hardness measurement used a load of 100 gf and a dwell time of 15 s. These measurements were taken at positions along the disc diameters separated by incremental distances of 0.3 mm and with the average hardness at each position estimated from four individual points recorded around the selected position and separated by distances of 0.15 mm. The grain structures in the HPT-processed Al–0.1% Mg alloy were examined by electron backscatter diffraction (EBSD) using a JSM6500F scanning electron microscope (SEM). For the initial as-annealed Al–0.1% Mg alloy, the microstructure was examined using a Wild M420 stereoscope.

The microstructures at the center and edge areas of the discs processed by 1/2 and 10 turns were studied by X-ray line profile analysis. The X-ray line profiles were measured with a high-resolution rotating anode diffractometer (Rigaku RA-MultiMax9) using $\text{Cu K}\alpha_1$ (wavelength, $\lambda = 0.15406$ nm) radiation. The 2D imaging plates detected the Debye–Scherrer diffraction rings. The line profiles were determined as the intensity distributions perpendicular to the rings obtained by integrating the 2D intensity distributions along the rings. The diffraction patterns were analyzed by the Convolutional Multiple Whole Profile (CMWP) fitting procedure^[43] to obtain the area weighted mean crystallite size ($\langle X \rangle_{\text{area}}$) and the dislocation density (ρ). In this method, the diffraction pattern is fitted by the sum of a background spline and the convolution of the instrumental pattern and the theoretical line profiles related to crystallite size and dislocations. In the calculation of the theoretical peak profile functions, it was assumed that the crystallite size distribution is log-normal. The instrumental peaks were measured on a LaB_6 line profile standard material (SRM 660).

Acknowledgements

This work was supported in part by the European Research Council under ERC grant agreement number 267464-SPDMETALS and in part by the Ministry of Human Capacities of Hungary within the ELTE University Excellence program (grant no. 1783-3/2018/FEKUTSRAT). One of the authors (Y.H.) thanks the QR fund from Bournemouth University.

Conflict of Interest

The authors declare no conflict of interest.

Keywords

Al–0.1% Mg alloys, hardness, high-pressure torsion, microstructures, X-ray

Received: December 27, 2019

Revised: February 6, 2020

Published online: February 24, 2020

- [1] R. Z. Valiev, R. K. Islamgaliev, I. V. Alexandrov, *Prog. Mater. Sci.* **2000**, 45, 103.
- [2] A. P. Zhilyaev, T. G. Langdon, *Prog. Mater. Sci.* **2008**, 53, 893.
- [3] C. Xu, Z. Horita, T. Langdon, *Acta Mater.* **2007**, 55, 203.
- [4] C. Xu, Z. Horita, T. Langdon, *Acta Mater.* **2008**, 56, 5168.
- [5] M. Kawasaki, S. N. Alhajeri, C. Xu, T. G. Langdon, *Mater. Sci. Eng. A* **2011**, 529, 345.
- [6] M. Kawasaki, R. B. Figueiredo, T. G. Langdon, *Acta Mater.* **2011**, 59, 308.
- [7] Y. Ito, Z. Horita, *Mater. Sci. Eng. A* **2009**, 503, 32.
- [8] K. Edalati, T. Fujioka, Z. Horita, *Mater. Sci. Eng. A* **2008**, 497, 168.
- [9] J. Wongsan-Ngam, M. Kawasaki, T. G. Langdon, *J. Mater. Sci.* **2012**, 47, 7782.

- [10] K. J. Al-Fadhalah, S. N. Alhajeri, A. I. Almazrouee, T. G. Langdon, *J. Mater. Sci.* **2013**, *48*, 4563.
- [11] Y. Huang, S. Sabbaghianrad, A. I. Almazrouee, K. J. Al-Fadhalah, S. N. Alhajeri, T. G. Langdon, *Mater. Sci. Eng. A* **2016**, *656*, 55.
- [12] Y. Huang, R. B. Figueiredo, T. Baudin, F. Brisset, T. G. Langdon, *Adv. Eng. Mater.* **2012**, *14*, 1018.
- [13] H.-J. Lee, S. K. Lee, K. H. Jung, G. A. Lee, B. Ahn, M. Kawasaki, T. G. Langdon, *Mater. Sci. Eng. A* **2015**, *630*, 90.
- [14] S. A. Alsubaie, Y. Huang, T. G. Langdon, *J. Mater. Res. Technol.* **2017**, *6*, 378.
- [15] A. P. Zhilyaev, Y. Huang, J. M. Cabrera, T. G. Langdon, *Defect Diffus. Forum* **2018**, *385*, 284.
- [16] J. Fu, H. Ding, Y. Huang, W. Zhang, T. G. Langdon, *J. Mater. Res. Technol.* **2015**, *4* 2.
- [17] K. Edalati, E. Matsubara, Z. Horita, *Metall. Mater. Trans. A* **2009**, *40*, 2079.
- [18] Y. Huang, M. Kawasaki, T. G. Langdon, *J. Mater. Sci.* **2013**, *48*, 4533.
- [19] Y. Cao, Y. B. Wang, X. H. An, X. Z. Liao, M. Kawasaki, S. P. Ringer, T. G. Langdon, Y. T. Zhu, *Acta Mater.* **2014**, *63*, 16.
- [20] A. Hohenwarter, A. Taylor, R. Stock, R. Pippan, *Metall. Mater. Trans. A* **2011**, *42*, 1609.
- [21] M. Kawasaki, R. B. Figueiredo, Y. Huang, T. G. Langdon, *J. Mater. Sci.* **2014**, *49*, 6586.
- [22] M. Kawasaki, *J. Mater. Sci.* **2014**, *49*, 18.
- [23] L. Radović, M. Nikačević, *Sci. Tech. Rev.* **2008**, *58* 14.
- [24] L. F. Mondolfo, in *Metallography of Aluminum Alloys*, Prentice-John Wiley and Sons Inc. New York **1943**, pp. 190.
- [25] G. B. Burger, A. K. Gupta, P. W. Jeffrey, D. J. Lloyd, *Mater. Charact.* **1995**, *35*, 23.
- [26] P. Bazarnik, B. Romelczyk, Y. Huang, M. Lewandowska, T. G. Langdon, *J. Alloys Compd.* **2016**, *688*, 736.
- [27] O. Andreau, J. Gubicza, N. X. Zhang, Y. Huang, P. Jenei, T. G. Langdon, *Mater. Sci. Eng. A* **2014**, *615*, 231.
- [28] Y. Huang, J. Millet, N. X. Zhang, P. H. R. Pereira, T. G. Langdon, *Mater. Sci. Forum* **2017**, *879*, 773.
- [29] G. E. Dieter, *Mechanical Metallurgy*, McGraw-Hill, Singapore, **1988**.
- [30] S. E. Ion, F. J. Humphreys, S. H. White, *Acta Metall.* **1982**, *30*, 1909.
- [31] T. C. Schulthess, P. E. A. Turchi, A. Gonis, T. G. Nieh, *Acta Mater.* **1998**, *46*, 2215.
- [32] R. Z. Valiev, Y. V. Ivanisenko, E. F. Rauch, B. Baudalet, *Acta Mater.* **1996**, *44*, 4705.
- [33] O. S. Sitdikov, R. O. Kaybyshev, I. M. Safarov, I. A. Mazurina, *Phys. Metals Metallog.* **2001**, *92*, 270.
- [34] D. P. Field, L. T. Bradford, M. M. Nowell, T. M. Lillo, *Acta Mater.* **2007**, *55*, 4233.
- [35] Q. He, T. Huang, L. Shuai, Y. Zhang, G. Wu, X. Huang, D. J. Jensen, *Scr. Mater.* **2018**, *153*, 68.
- [36] Y. H. Zhao, J. F. Bingert, T. D. Topping, P. L. Sun, X. Z. Liao, Y. T. Zhu, E. J. Lavernia, *Mater. Sci. Eng. A* **2020**, *772*, 138706.
- [37] R. B. Figueiredo, P. H. R. Pereira, M. T. P. Aguilár, P. R. Cetlin, T. G. Langdon, *Acta Mater.* **2012**, *60*, 3190.
- [38] P. H. R. Pereira, R. B. Figueiredo, *Mater. Trans.* **2019**, *60*, 1139.
- [39] P. H. R. Pereira, R. B. Figueiredo, Y. Huang, P. R. Cetlin, T. G. Langdon, *Mater. Sci. Eng. A* **2014**, *93*, 185.
- [40] K. Edalati, Y. Hashiguchi, P. H. R. Pereira, Z. Horita, T. G. Langdon, *Mater. Sci. Eng. A* **2018**, *714*, 167.
- [41] M. Y. Alawadhi, S. Sabbaghianrad, Y. Huang, T. G. Langdon, *Adv. Eng. Mater.* **2019**, <https://doi.org/10.1002/adem.201901015>.
- [42] R. B. Figueiredo, P. R. Cetlin, T. G. Langdon, *Mater. Sci. Eng. A* **2011**, *528*, 8198.
- [43] G. Ribárik, J. Gubicza, T. Ungár, *Mater. Sci. Eng. A* **2004**, *387–389*, 343.